Molecular Dynamics simulation based investigation of possible enhancement in strength and ductility of nanocrystalline aluminum by CNT reinforcement

Snehanshu Pal, Pokula Narendra Babu, B.S.K. Gargeya, Charlotte Becquart

Molecular Dynamics Simulation Based Investigation of Possible Enhancement in Strength and Ductility of Nanocrystalline Aluminum by CNT Reinforcement

Snehanshu Pal[a*], Pokula Narendra Babu[a], B.S.K. Gargeya[a,b], Charlotte S. Becquart[c]

[a]Department of Metallurgical and Materials Engineering, National Institute of Technology Rourkela, Rourkela - 769008, India

[b]Department of Materials Engineering, Indian Institute of Science, Bangalore - 560012, India

[c]Univ. Lille, CNRS, INRA, ENSCL, UMR 8207 - UMET - Unité Matériaux et Transformations, F-59000 Lille, France

*Corresponding author: Snehanshu Pal E-mail address:snehanshu.pal@gmail.com; pals@nitrkl.ac.in.Phone No. +91-661-2462573.

Abstract

Molecular dynamics (MD) based study of nanocrystalline (NC) Al and CNT (carbon nanotube) reinforced NC Al specimens having grain sizes ~9 nm have been carried out under tensile loading using hybrid potentials for different temperatures (10 K, 300 K and 681 K) at a particular strain rate of $10^{10}\,\text{s}^{-1}$. Structural variation and defect evolution during the deformation have been investigated. An enhancement in both strength and ductility is observed in case of the CNT embedded NC Al specimens with respect to NC Al specimen and such improvement is significant in case of (30,30) CNT embedded NC Al specimen. It is also found that NC Al matrix is fractured first, then the CNT at lower test temperature, whereas at high temperature, the CNT fractures before the matrix.

Keywords: Molecular dynamics; Nanocrystalline materials; Carbon nanotubes; Tensile loading.

Introduction

Reduction in grain size of polycrystalline metal into nano scale more precisely less than 100 nm has positive influence on mechanical properties like strength [1] and hardness [2] and thereby nanocrystalline (NC) metals have attracted a great deal of attention [3-7]. However, low ductility (~5-8%) remains to be a drawback of such materials; therefore these materials are not able to gain deserved importance as structural materials [8, 9]. Moreover, a rise in strength as well as in ductility for nanostructured metallic systems is mutually exclusive [10, 11]. In this regard, Carbon Nanotubes (CNTs) reinforcement may play a vital role as they possess a low density (~1.2g/cm^3), a high tensile strength (~100 GPa), a high Young's modulus (~900 GPa) and a tensile ductility of ~20%. Moreover, CNTs already attract a lot of attention as promising materials in various fields such as sensors [12], energy applications [13], biomedical applications [14], polymer composites [15, 16]. Successful attempt to exploit mechanical properties of CNT has been demonstrated enormously in the case of CNT reinforced polymer composites with improved tensile strength [17], flexural strength [18] and fatigue resistance [19, 20]. This has led to the experimentation of reinforcing metals (polycrystalline and Nanocrystalline) with CNTs, thereby producing "Metal Matrix Composites" (MMCs), a new class of composites to achieve a combination of enhanced strength and ductility [21, 22]. Shi et. al [23] have experimentally investigated the mechanical properties of Single Walled Carbon Nanotube (SWCNT)-Aluminium composites using microscopic tensile tests and reported improvement in strength without compromising on ductility. Compression studies suggested that a combined effect of CNT reinforcement and grain refinement contributed to the improved strength. Hou et. al [24] have reported increased strength of 355 MPa and ductility (~15%) in Mg-9Al alloys reinforced with Multi Walled CNTs (MWCNTs). In-situ formation of nanoscale Mg$_{17}$Al$_{12}$ phase using the MWCNTs as a heterogeneous nucleation site. However, in order to achieve these benefits in a more systematic, reliable and reproducible manner, (1) proper

fabrication of these composites with respect to homogeneous dispersion of CNTs in the matrix [25], (2) a proper understanding of the matrix-CNT interface structure, and (3) load transfer across the interface needs to be clearly understood. Experimental methods such as Molecular Level Mixing (MLM) [26] and Mechanical Alloying [27] have been successful in achieving homogeneous dispersion of CNTs. This indicates a progress in the direction of factor (1) mentioned above. However, with respect to the length and time scales controlling the factors (2) and (3), an experimental approach to address these factors would be very tedious, costly and time consuming, if not impossible. In this regard, Molecular Dynamics (MD) simulations based investigation can be beneficial for studying deformation behaviour at the atomic scale [28, 29]. For instance, the mechanical properties (toughness and Young's modulus) of CNT reinforced single crystal (SC) Al composites is found to be enhanced and CNTs restrict the fracture of the composite by bearing extreme load [30]. The mechanical properties of such material are influenced by diameter and chirality of CNT [31] and the rate of CNT reinforcement [32]. Silvestre et. al [33] have performed compressive studies on Aluminium Single crystal-CNT composite measuring 4.85 nm x 4.85 nm x 10.22 nm, and observed slip bands at 45°. Also, premature failure of the composite was attributed to buckling of CNT. Duan et. al [34] have performed MD simulations to understand the damping behaviour of Ni coated CNT – Copper composite at a temperature of 300 K and found out that the distorted Cu lattice at the interface was responsible for the dissipation of energy. Chen et al. stated that the improvement of the ductility and strength of CNT/Al composites is due to boosting up the bonding conditions between matrix and reinforcement [35]. Although the above studies show possible enhancement of mechanical properties of Al by CNT reinforcement, detailed atomic level studies of mechanical behaviour and corresponding underlying mechanisms of NC Al by CNT reinforcement have not been studied till date. In this paper, the mechanical behaviour and fracture mechanisms of CNT embedded NC Al composite have been investigated using MD

simulations under uniaxial tensile loading condition. The effect of CNT diameter as well as the impact of temperature on the deformation behaviour of the composite subjected to tensile load has also been studied.

Simulation details

The 20×20×20 nm^3 NC Al specimens (each contains 12 grains with a grain size of 9 nm) have been created by the Voronoi method [36] using the Atomsk software [37]. In the present study, armchair-CNTs with (5,5), (15,15), (30,30) have been constructed, then inserted into the NC-Al specimens (**Fig. 1(a)**). MD Simulation studies by Choi et. al on single crystal Al/CNT composites at 300 K have shown to reach UTS at a strain of 0.18 and fracture strain of 0.45 [30], whereas in the present study (for the 300 K case), the UTS of NC Al with (5,5) CNT is reached at a strain of 0.14 and fracture strain of at least 0.84. The deviation suggests that the position of the CNT with respect to grains and grain boundaries (GBs) affect the properties. However, due to our specimen size, it is not possible to complete such a study. The CNTs in this work pass through grains and grain boundaries. The x, y, z orientations are [100], [010] and [001] respectively. The number of atoms in NC Al without CNT, NC Al of (5,5) CNT, NC Al of (15,15) CNT and NC Al of (30,30) CNT is 483274, 486641, 488252 and 490096. The smallest diameter of the CNTs used in this work is 0.678 nm. The radius of the aluminium atom is 0.184 nm, which suggests a possibility of introducing aluminium atoms inside the CNT. In fact, the absence of matrix atoms in the CNT would represent a system in which the deformation processes (dislocation generation and annihilation, fracture) would be biased to the matrix-CNT interface, and would not represent a typical behavior. Previously carried out tensile deformation simulations of single crystal Al/CNT composites keeping CNT cores empty, showed that void generation occurred at the matrix-CNT interface and that the hole in the centre of the CNT weakened the composite [30]. Hence, in order to get rid of such bias, the inner part of the CNT, in our study, is filled with aluminium atoms. Periodic boundary

conditions have been applied in the X, Y, and Z directions and the time step was taken as 0.001 ps. An Embedded Atom Method (EAM) potential [38] and an Adaptive Intermolecular Reactive Empirical Bond Order (AIREBO) potential [39] have been applied for Al-Al and C-C interactions respectively. The EAM computes the total energy E_i as

$$E_i = F_\alpha \left(\sum_{j \neq i} \rho_\beta(r_{ij}) \right) + \frac{1}{2} \sum_{j \neq i} \emptyset_{\alpha\beta}(r_{ij})$$

Where F is the embedding energy (depends on atomic electron density ρ), Φ is the pair potential function, α and β are the element types of atoms i and j. The AIREBO style computes the energy as

$$E = \frac{1}{2} \sum_i \sum_{j \neq i} \left[E_{ij}^{REBO} + E_{ij}^{LJ} + \sum_{k \neq i,j} \sum_{l \neq i,j,k} E_{kijl}^{TORSION} \right]$$

The Al-C interaction is modelled with a Lennard-Jones (LJ) 12-6 potential based on the van der Waals forces [40]. The preferred cutoff distance is taken as 10.2 Å, which is three times larger than that of the C-Al interaction in order to fit to the cutoff distance of the AIREBO potential [30]. The Lennard-Jones (LJ) 12-6 is computed as

$$E = 4\epsilon \left[\left(\frac{\sigma}{r} \right)^{12} - \left(\frac{\sigma}{r} \right)^6 \right]$$

Where E is intermolecular potential among the Al and C atoms, σ is the distance at which the inter-atomic potential is zero, r is the distance between two atoms, and ϵ is the potential well depth. Energy minimization was performed using the conjugate gradient method and subsequent equilibration was done at 10 K, 300 K, and 681 K (~0.7*Melting point) using the NPT ensemble. The equilibration was performed for 20000 time steps. Then the specimens were subjected to a uniaxial tensile loading in the Z-direction in the NVT ensemble [30, 31] at a strain rate of 10^{10} s^{-1}. Although the strain rate used is not similar to experimental strain rates, this work will provide insights into the underlying atomistic mechanisms of CNT reinforced

NC Al metal matrix nanocomposites during the deformation process. Furthermore, in order to check the impact of the strain rate, one representative simulation was done at a lower strain rate of 10^9 s^{-1} at 300K.The MD simulations were performed with LAMMPS [41] and the post processing done using OVITO software [42]. The dislocation density and their types have been investigated using the dislocation analysis (DXA) [43]. Presence of Stacking faults can be identified using the Common Neighbor Analysis technique (CNA) [44]. The atomic strain tool of OVITO [45, 46] has been used to find out the shear strain distribution in the matrix and CNT during the deformation. The vacancies have been analysed using the Wigner-Seitz defect analysis tool of OVITO. The spatial distribution of vacancies has been obtained by retaining only those sites whose "Occupancy" was reported as zero by OVITO.
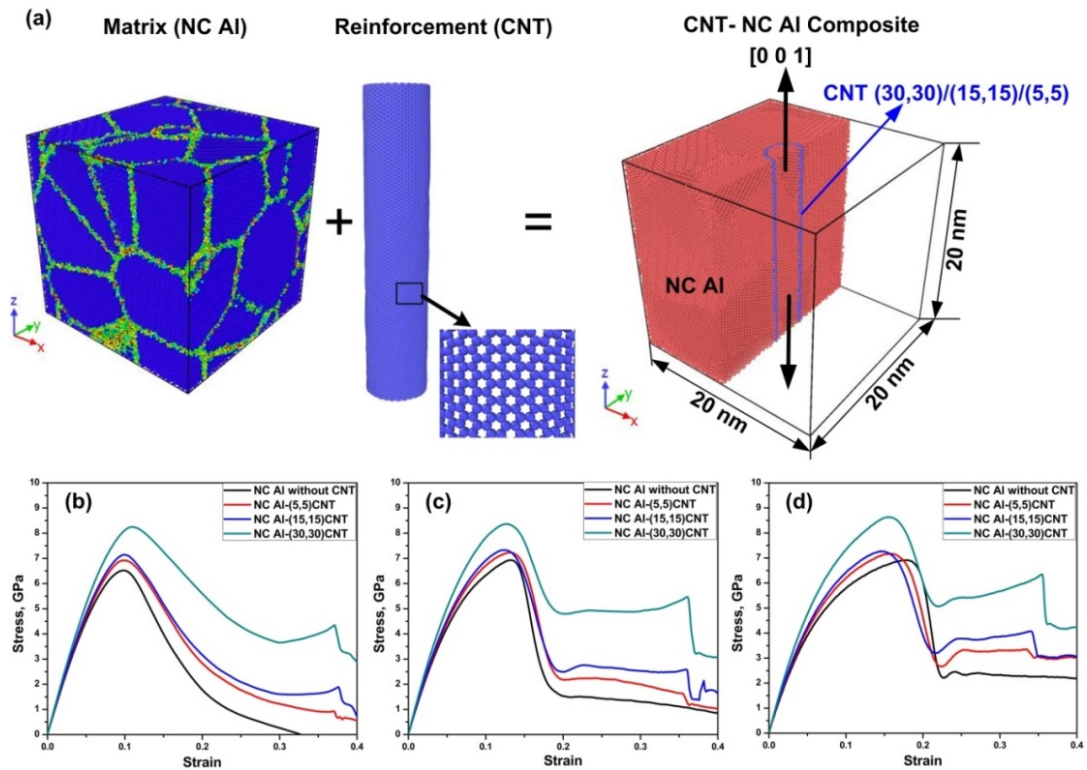
Results and discussion

Fig. 1. (a) Initial specimen of CNT-NC Al composite (Composite generated from the combination of NC Al represented in Centrosymmetry parameter analysis and a CNT which

has been inserted in the hole created in the matrix) and Stress-strain plots of NC Al without CNT and CNT reinforced NC Al specimens at different temperatures (b) 10 K (c) 300 K (d) 681 K.

Stress-strain plots of the NC Al and NC Al-CNT specimens for different temperatures are presented in **Fig. 1** and the evaluated mechanical properties are summarized in **Table 1**. Young's modulus was calculated by using a linear regression analysis and the yield strength by the 0.2% offset method, and the detail of the method is available in the literature [30, 47]. Both, Young's modulus and yield strength are found to increase when the CNT diameter increases at all temperatures. It is also seen that the percentage of modulus improvement (for the NC Al-(30,30) CNT compared against the NC Al without CNT) is ~14% at 10 K, ~15% at 300 K and reaches the highest value of ~21.5% at 681 K, thereby indicating that the enhancement of modulus is higher at higher temperatures. However, an opposite trend is observed for the case of yield stress. The percentage improvement in yield strength (for the NC Al-(30,30) CNT compared against NC Al without CNT) is ~34% at 10 K, ~28% at 300 K and ~20% at 681 K. Regarding the impact of temperature, the modulus and yield strength is found to decrease when the temperature increases. Conversely, the opposite tendency is observed for the Ultimate Tensile Strength (UTS). It can be seen from the stress-strain plots that the stress drops continuously beyond the UTS for NC Al without CNT specimen, at all the temperatures considered here. However, the stress increases slightly in the regime beyond the UTS for the NC Al-CNT nano-composites, and this behaviour becomes more pronounced for the composite specimen with the higher CNT diameter. This behaviour is attributed to the contribution of the matrix to the total stress which is higher at lower strains due to a higher volume fraction, and the contribution of CNT to the total stress which is higher at higher strains due to its higher strength. In other words, the stress strain plots of the matrix and the CNT follow the rule of mixtures.

Table 1. Mechanical properties of NC Al and CNT reinforced NC Al composites for different temperatures.

Specimens	Young's Modulus (GPa)			Yield Strength (GPa)			Ultimate Tensile Strength (GPa)			Fracture Strain		
	10 K	300 K	681 K	10 K	300 K	681 K	10 K	300 K	681 K	10 K	300 K	681 K
NC Al without CNT	100.9	97.8	91.3	3.2	3	2.9	6.52	6.93	6.91	0.56	1.02	1.31
NC Al with (5,5) CNT	104.1	101	100	4.1	3.15	2.98	6.92	7.24	7.17	0.73	0.84	1.51
NC Al with (15,15) CNT	105.6	104	102	4.2	3.4	3.12	7.14	7.33	7.28	0.63	1.01	1.71
NC Al with (30,30) CNT	115.2	113	111	4.3	3.85	3.5	8.25	8.37	8.64	0.88	1.59	2.2

Table 2. Mechanical properties at 300 K calculated using MD simulations for NC Al and CNT reinforced NC Al composites having different grain size.

Specimens	Grain size (nm)	Ultimate tensile strength (GPa)	Fracture strain
NC Al without CNT	4	8.25	1.24
NC Al with (30,30) CNT	4	8.93	1.42
NC Al without CNT	6	7.68	0.81
NC Al with (30,30) CNT	6	8.46	1.31
NC Al without CNT	9	6.93	1.02
NC Al with (30,30) CNT	9	8.37	1.59

The effect of grain sizes on mechanical properties of NC Al and CNT reinforced NC Al composites at 300 K are displayed in **Table 2**, and the corresponding stress-strain plots in **Fig. S2**. The ultimate tensile strength is the highest for the smallest grain size studied. In general, our study shows that increasing the grain size leads to a decrease of the mechanical properties, which is in line with the findings reported in literature [48, 49]. In most engineering applications where strength is an important factor, the toughness is often an issue. **Fig. 2** compares the UTS and fracture strain achieved by CNT reinforcement. It can be seen that the addition of CNTs with ((5,5) and (15,15)) led to only minor improvements in the UTS, and

minor changes in the fracture strain. However, the addition of (30,30) CNT induce a significant improvement in both UTS and fracture strain, thereby indicating a higher toughness, evident at all the considered temperatures.
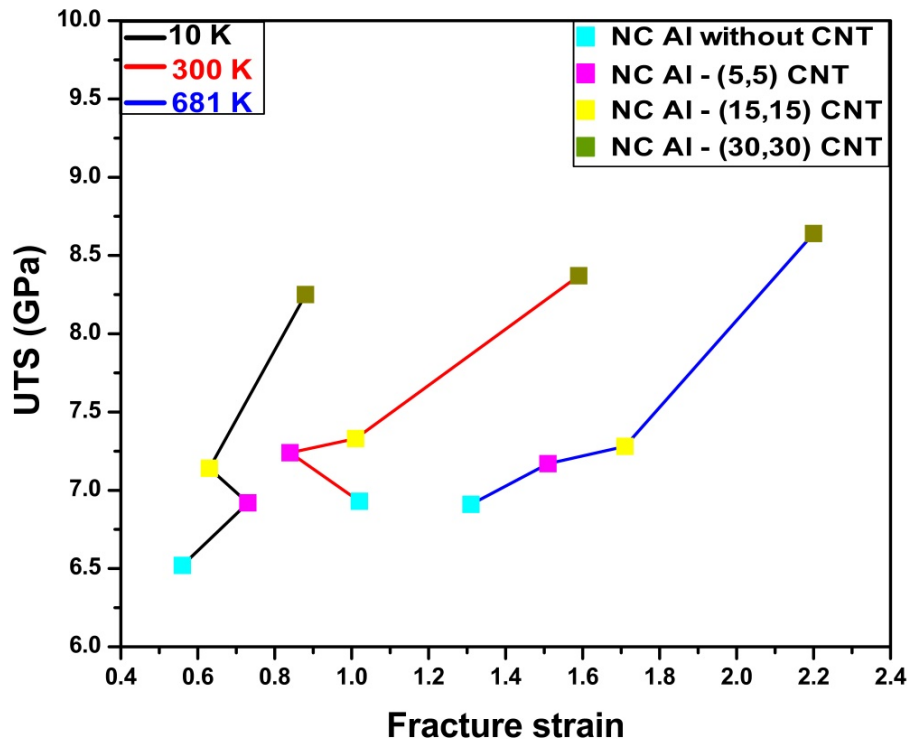

Fig. 2. (a) Ultimate tensile strength vs. fracture strain plot showing NC Al without CNT and CNT reinforced NC Al specimens at various temperatures 10 K, 300 K and 681 K.

Table 3. Volume fraction of (5,5) CNT, (15,15) CNT and (30,30) CNT

Chirality	Volume fraction (in %)
(5,5)	0.075
(15,15)	0.224
(30,30)	0.448

The different CNT volume fractions investigated in this work are displayed in **Table 3**, and the properties of the nanocomposites with these CNT volume fractions are shown in **Fig.3**. In that figure, red, green, blue and cyan colours indicate respectively the 0 vol.% (i.e. without CNT), 0.075 vol.%, 0.2 vol.% and 0.4 vol.% CNT content. The material properties such as Young's modulus as well as the yield strength increase with the CNT volume fraction according to **Fig.3**,

9

which is also seen in previously reported works [50-53]. In addition to this, the load bearing capacity, the UTS and fracture strain of the composite are also enhanced with an increase in the CNT volume fraction, in agreement with literature [54, 55].
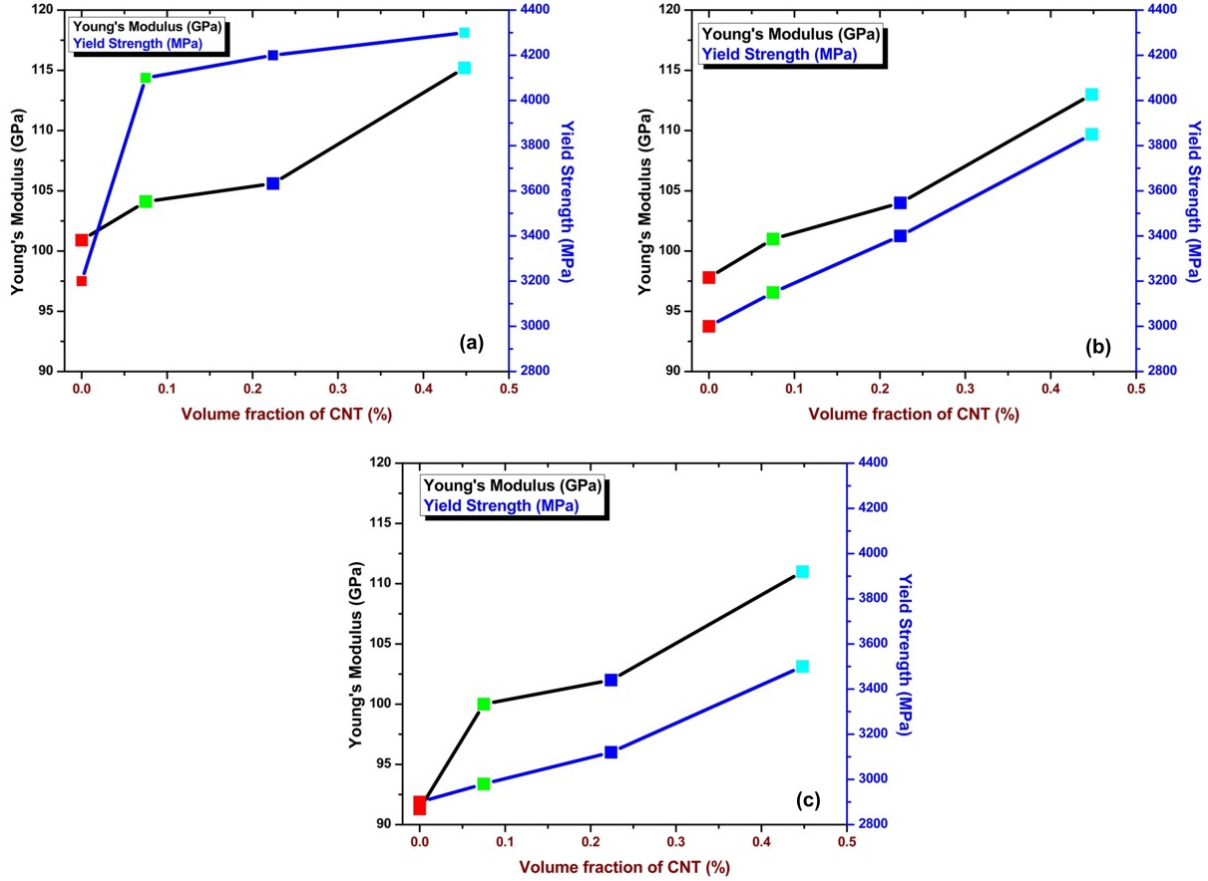

Fig. 3. Mechanical properties for varying CNTs volume fraction at (a) 10 K, (b) 300 K, and (c) 681 K.

Fig. 4 illustrates the stress-strain plots of the NC Al and NC Al-CNT specimens for 300 K at a 10^9 s^{-1} strain rate. The stress-strain plots at 10^9 s^{-1} exhibit a lower ultimate tensile strength values and a sudden drop in strength after UTS in comparison with the stress-strain plots at 10^{10} s^{-1}. However the behavior of the different specimens studied on the basis of mechanical properties such as Young's modulus, yield strength and UTS remain the same.
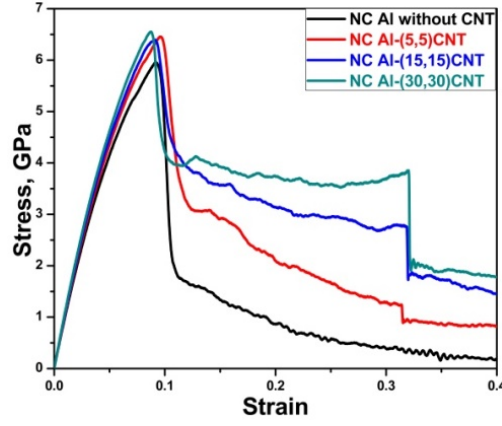
Fig. 4. Stress strain plots of the NC Al with and without CNTs at 300 K for a 10^9 s^{-1} strain rate.
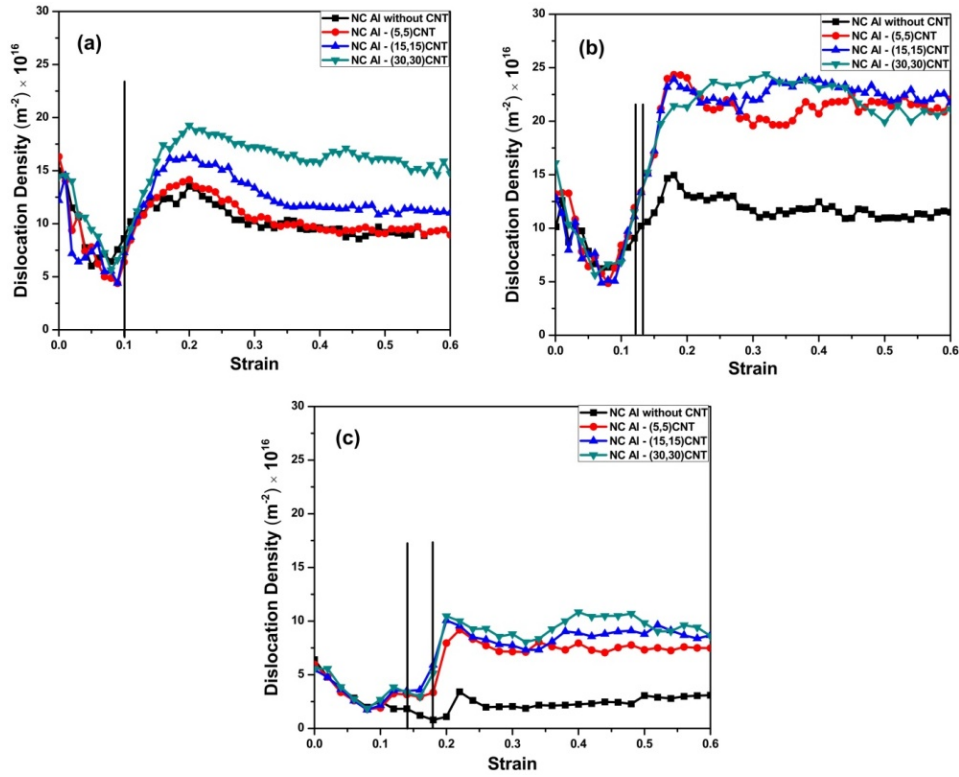

Fig. 5. Plots of overall dislocation densities vs. strain for NC Al without CNT and CNT reinforced NC Al specimens at various temperatures (a) 10 K, (b) 300 K and (c) 681 K.

The mechanical behaviour of materials can very often be explained by the behaviour of their defects. Addressing this, we plotted the dislocation density evolution during the tensile deformation for all the cases in **Fig. 5(a-c)**. A common trend is observed: the dislocation density decreases first, and then increases gradually to reach a steady state at the end of the deformation process. Note that dislocations do exist in the grain boundaries of the sample prior

to loading. Loading makes these dislocations move towards the specimen surfaces, thereby leading to the decrease of the dislocation density, in the initial stages of the loading. Although there is also generation of dislocations in the initial stages of deformation, the annihilation rate of these dislocations at the surface dominates the rate of dislocation generation. At further stages of loading, the dislocation generation is significantly higher, and the dislocation density increases. The vertical black lines marked on the plots indicate the strain at UTS (which is found to vary with CNT diameter. It can be seen that the increase in dislocation density beyond UTS point is higher for NC Al composites with higher CNT diameter and at higher temperatures (refer **Fig. 5(a-c)**). The test temperature is also seen to have a pronounced effect on the dislocation density. At lower temperatures such as 10 K, (**Fig. 5(a)**) the dislocation density is less than that expected from strain hardening theory. According to strain hardening theory, a higher strength at low temperature is expected due to a lower rate of dislocation annihilation, assuming that the production of dislocations is not difficult. This assumption may not be valid at low temperatures such as 10 K where the atomic movement is difficult. Therefore, the two factors, namely, (1) a low mobility of atoms, and (2) a high strength of grain boundaries render dislocation generation difficult. In conventional polycrystalline materials with grain sizes ~μm, dislocations are generated through sources such as Frank-Read sources. However, in NC materials, such sources do not exist for two reasons: 1. The small sized ~nm grains cannot contain the dislocations due to their inability to bear the distortion of the lattice caused due to dislocation due to higher strains (the strain is proportional to b/d, where b is the burgers vector and d is the grain size). 2. The proximity of grain boundaries (which can act as a surface) attracts the dislocations towards themselves (via image dislocations). The force image is F_{image} = -Gb^2/ (4*pi*(1-v)*d), d = distance between the dislocation and the free surface, v = Poisson's ratio [56]. Apart from the above two reasons, evidence of dislocations emanating from GBs in nanocrystalline materials has been reported widely in literature [57,

58]. In this study, the dislocations are initiated from the grain boundaries of the NC materials (Fig. **S1**). In nanocrystalline materials, since the grains boundaries are the main source of dislocations, their inability to produce dislocations would reduce the overall dislocation density. As the temperature increases to 300 K, the dislocation density increases due to above mention reasons. At even higher temperatures such as 681 K, dislocation annihilation takes place, thereby reducing the dislocation density. From our results in **Fig. 5**, it can be seen that the dislocation density is higher for the CNT reinforced NC Al as compared to NC Al and this is more pronounced at higher temperatures. It can also be said that CNT hinders dislocation movement owing to the mismatch between the matrix and the CNT particles at the interface. Xiang et al. and Lu et al. have showed that interfacial shear stresses (interactions) depend on the CNT chirality and interaction perimeter [31, 59].
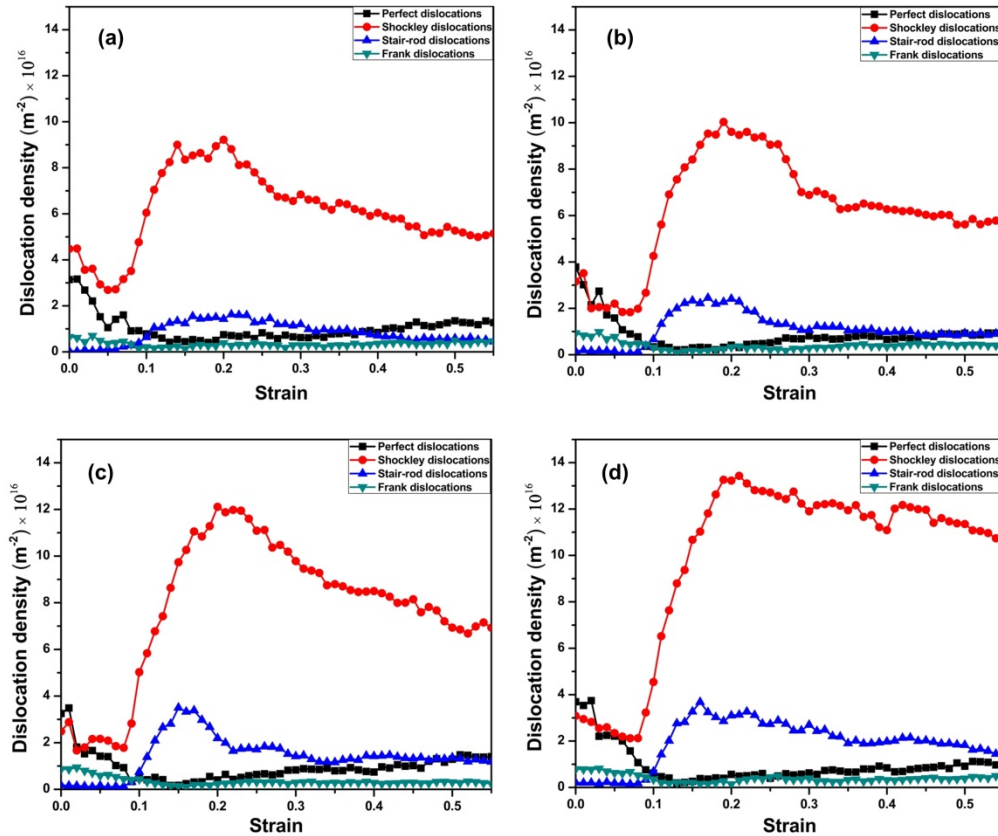

Fig. 6. Plots showing types of dislocations for (a) NC Al without CNT, (b) (5,5) CNT, (c) (15,15) CNT and (d) (30,30) CNT reinforced NC Al specimens at 10 K temperature.

A detailed analysis of the dislocation density for each type of dislocations is depicted in **Fig. 6**. Four types of dislocations, namely perfect, Shockley partial, Frank partial and stair-rod have been analyzed as they are of prime importance for the mechanical behaviour. **Fig. 6** represents the dislocation density at 10 K. Comparing **Fig. 6(a)** with **6(b), 6(c)** and **6(d)**, it can be inferred that reinforcing NC Al with CNT favours the formation of Shockley and stair-rod dislocations. In the initial stages of deformation, the density of both Shockley partials and stair-rod dislocations are seen to first remain almost constant, then they increase suddenly at a particular strain and finally they reduce at around 17-22% strain where, a drop in these densities is observed. Not much variation in the dislocation density is observed for the Perfect and Frank partial dislocations as a function of CNT diameter. The dislocation densities decrease in the initial stages of deformation, and then remain constant. The results of the dislocation density variation at 300 K are qualitatively similar to the case of 10 K, excepting that the density of perfect dislocations increases slightly in the later stages of deformation (see **S3**). The stair-rod and Frank dislocations are entirely absent in case of 681 K (see **S4**). The deformation happens thus predominantly by Shockley partials and to a minor extent by perfect dislocations. This is because, at high strain rates, the stresses achieved are well above the critical stress required to initiate the partial dislocation activity. The critical stress τ is dependent on the intrinsic stacking fault energy γ and the burgers vector b. In order to prevent the stacking fault from collapsing, the work done must exceed γ, i.e. $\tau > \gamma/b$. The stresses in the present studies are well above ~1 GPa, hence partial dislocations (manifested as Stacking Faults) are dominant, as most of the perfect dislocations are expected to have dissociated into partials in agreement with literature [60, 61].
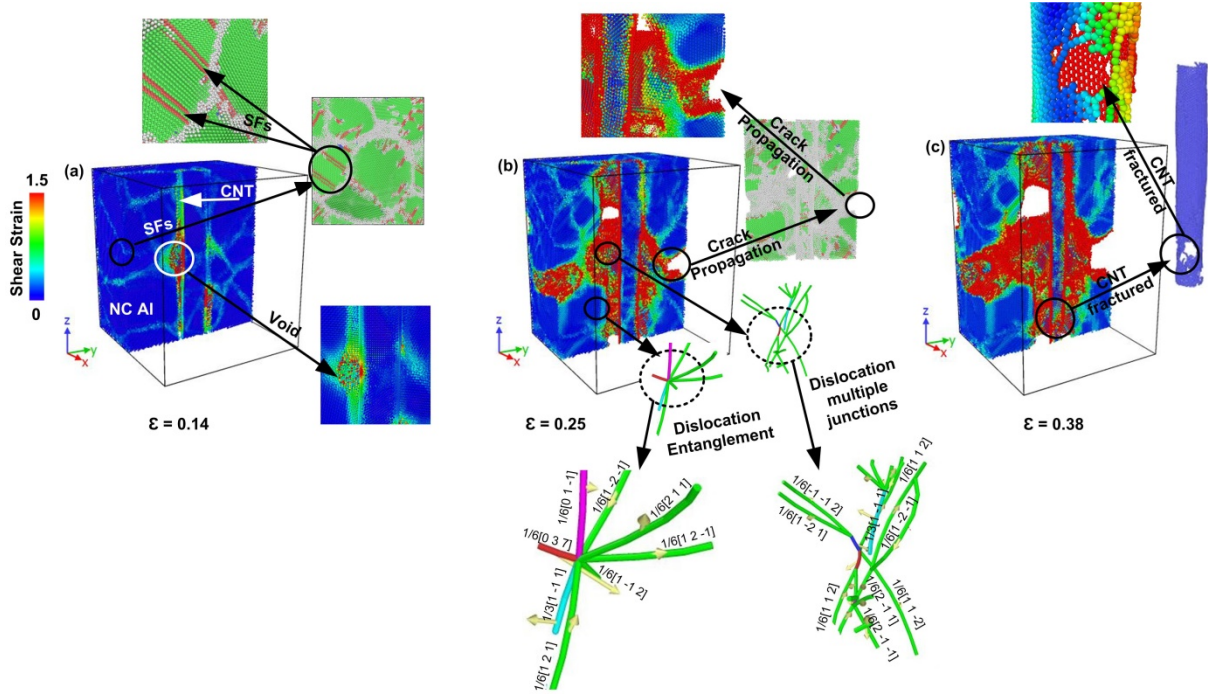
Fig. 7. Atomic strain snapshots of (30,30) CNT reinforced NC Al specimens during tensile deformation process in slice vision at 10 K temperature. (a) Void and stacking faults formation (inset through common neighbor analysis), (b) Crack propagation and representation of dislocations and (c) CNT fracture.

Fig. 7 shows the atomic snapshots of the various features influencing the deformation in NC Al with (30,30) CNT at 10 K. (Similar results have been observed for (5,5) and (15,15) diameters. Refer to Supplementary Figures). The atoms are coloured according to the shear strain. It can be seen from **Fig. 7(a)** that at 14% strain, the failure of the composite is initiated by void generation at the interface between the grain boundary of the matrix and CNT. Common Neighbour Analysis pictures also suggest the formation and propagation of stacking faults (Coloured as orange bands, and indicated using arrow marks). The shear strain distribution within the CNT and matrix is uniform. **Fig. 7(b)** shows the dislocation type and structure at the vicinity of the cracks. Dislocation entanglement and dislocation multiple junctions are seen to form. Although the Shockley partials are more numerous, Frank partials and stair-rod dislocations are also observed. The Burgers' vector and dislocation line direction suggest that both edge and screw dislocations are present. Note also that the morphology of the

CNT indicates that the CNT bears no cracks, which suggests matrix cracking as the mechanism of failure of the composite. This is an expected mechanism at such low temperatures due to the extremely low ductility of metals at such temperatures. The cracks are seen to propagate along the grain boundaries via void amalgamation. **Fig. 7(c)** shows the morphology of the matrix and CNT at 38% strain, where the CNT is found to fracture. Inhomogeneity in shear strain to some extent is observed within the matrix and CNT.
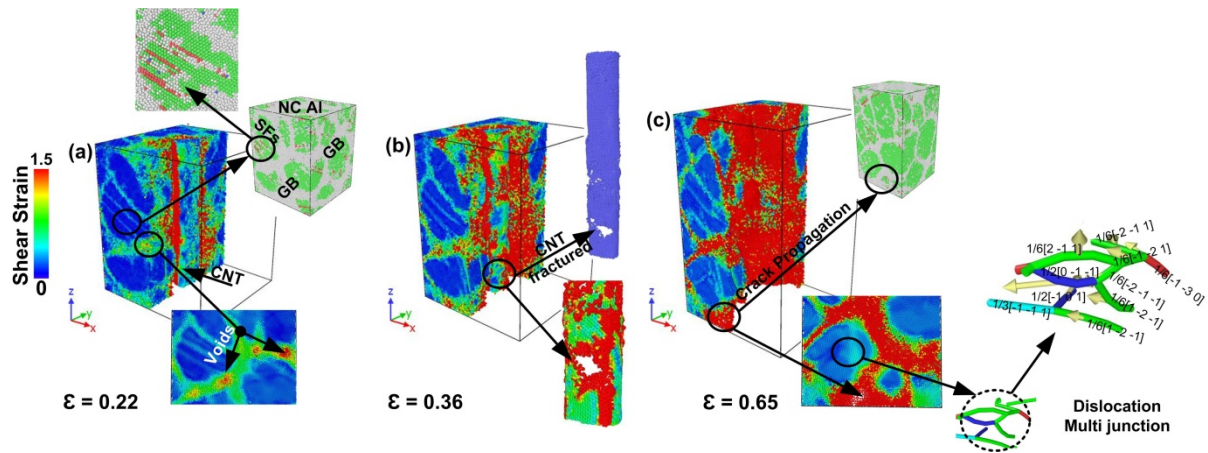

Fig. 8. Atomic strain snapshots of (30,30) CNT reinforced NC Al specimens during tensile deformation process in slice vision at 681 K temperature. (a) Void and stacking faults formation (inset through common neighbor analysis), (b) Crack propagation and representation of dislocations and (c) CNT fracture.

Fig. 8 shows the atomic snapshots of the various features influencing the deformation in NC Al with (30,30) CNT at 681 K. It can be seen from **Fig. 8(a)** that at 22% strain, the voids begin to form. A comparison of **Fig. 8(a)** with **Fig. 7(a)** suggests that the grain boundary has thickened at higher temperatures (as can be deduced from the Common Neighbour Analysis snapshots). Furthermore, the shear strain distribution is seen to be non-uniform even at lower values of strain. **Fig. 8(a)** indicates that the regions of CNT in contact with the aluminum lattice have higher shear strains, and the regions of CNT in contact with the GBs of NC Al have lower shear strains. **Fig. 8(b)** shows the snapshots at a strain of 36%, where the CNT fracture is initiated. Significant inhomogeneity in the strain distribution has been attained, and fracture is

seen to occur in regions with higher strains. **Fig. 8(c)** shows the snapshot at a strain of 65%, when the matrix begins to crack. Unlike the 10 K case, the failure of the composite is initiated by fibre breakage, and continued by matrix cracking. This is expected at higher temperatures due to the increased ductility of the matrix, and relatively brittle nature of the CNT reinforcement. The Burgers' vector and type of dislocations are also indicated in **Fig. 8(c)**. Shockley partials, Stair-rod and perfect dislocations are seen at the vicinity of the crack. A majority of the dislocations happen to be either edge or mixed type of dislocations. This is because the screw dislocations having a high mobility, move quickly in response to the applied load, and thus get annihilated at the grain boundaries or at the surfaces. The overall set of events: void formation, crack propagation at the grain boundary, and CNT fracture is observed during the tensile deformation of all the CNT reinforced specimens.
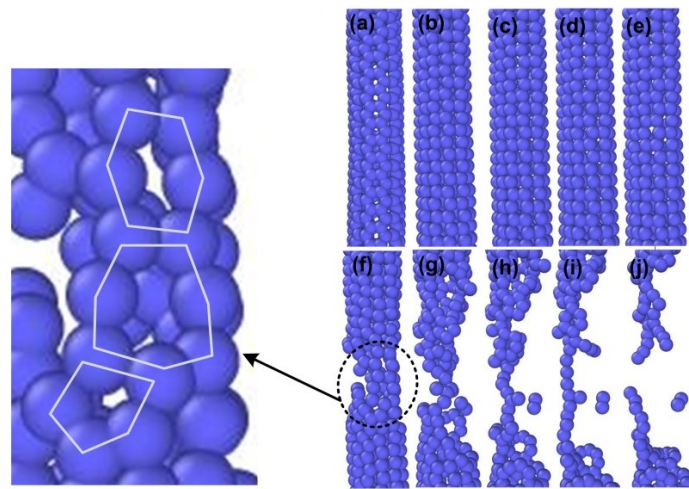

Fig. 9. Atomic snapshot representations of (5,5) CNT fracture path for 10 K during tensile deformation process.

Fig. 9 shows the mechanism of CNT failure for (5,5) CNT at 10 K. It can be seen that the mechanism of failure is almost the same for all diameters. "Fibre" like appearance suggests that the bonds are broken by shear failure. i.e., rupture of bonds takes place. **Fig. 9(e)** shows the disrupted order of atoms from where the failure has been initiated. The point of CNT rupture is seen to be the same point where the voids developed in the Al matrix. Another mechanism

is the formation of Stone-Wales defect which is reported to reduce the strength of the CNTs, thereby making them prone to failure, as found in the literature [30]. An observation of the CNT morphology in **Fig. 9(f)** shows the regions in which the rings are distorted from hexagonal shapes to rings with five and seven carbon atoms (these are the so-called Stone Wales defects). These defects are known to induce distortion in the bonds and bond angles, and become sites of failure initiation and rapid propagation as previously reported by Lu and Bhattacharya [62]. A similar fracture mechanism has been observed for (15,15) CNT and (30,30) CNT (**S12**).
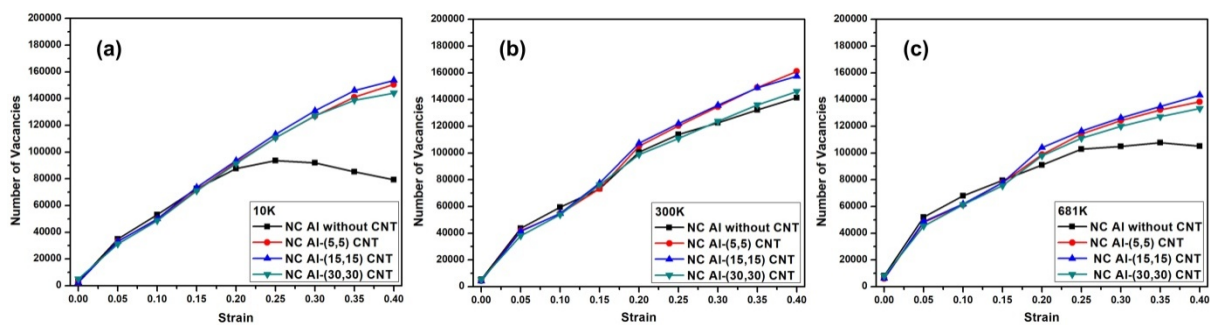

Fig. 10. Plots of the number of vacancies vs. strain for NC Al without CNT and CNT reinforced specimens at various temperatures (a) 10 K (b) 300 K and (c) 681 K.

While details regarding dislocations and shear strain distribution provide information on the deformation behaviour of materials, vacancies also play a role, particularly at high temperatures due to their increased concentration and increased mobility. In nanocrystalline materials, easy diffusion paths such as grain boundaries are extensively available, and hence vacancy motion becomes important. **Fig. 10** shows the variation of the total number of vacancies as a function of strain for our specimens at (a) 10 K, (b) 300 K and (c) 681 K. It can be seen from all the three figures that the vacancies are produced as the deformation progresses. At temperatures 10 K and 681 K, the NC Al is seen to have a reduced number of vacancies at later stages of deformation. As far as the CNT diameter is concerned, its effect on the number of vacancies is not so significant at all the temperatures investigated here. However, the effect of CNT diameter on the vacancies can be better understood by the spatial distribution of

vacancies along the x-direction as represented in **Fig. 11**. It is observed that the vacancy concentration is higher at the matrix-CNT interface compared to the region away from the interface. The "interface" in this context refers to the region up to either ends of the CNT. More precisely, in our description, the specimen is centered at 0, and the interface is the region situated close to x = -R to x = +R, where R is the radius of the CNT. The ratio of the average number of vacancies at the interface to the number of vacancies away from the interface can be seen to be more or less unaffected with changes in temperature. The CNTs with higher CNT diameter tend to attract more number of vacancies at the interface. As deformation progresses, the vacancy pile up at the interface is destroyed, and the distribution of vacancies is uniform across the specimen. This is expected to happen via grain boundary diffusion of vacancies (at low temperatures such as 10 K) and via lattice diffusion as well (at high temperatures such as 681 K), as reported in the literature [63]. Apart from this, additional vacancies are produced during the deformation.
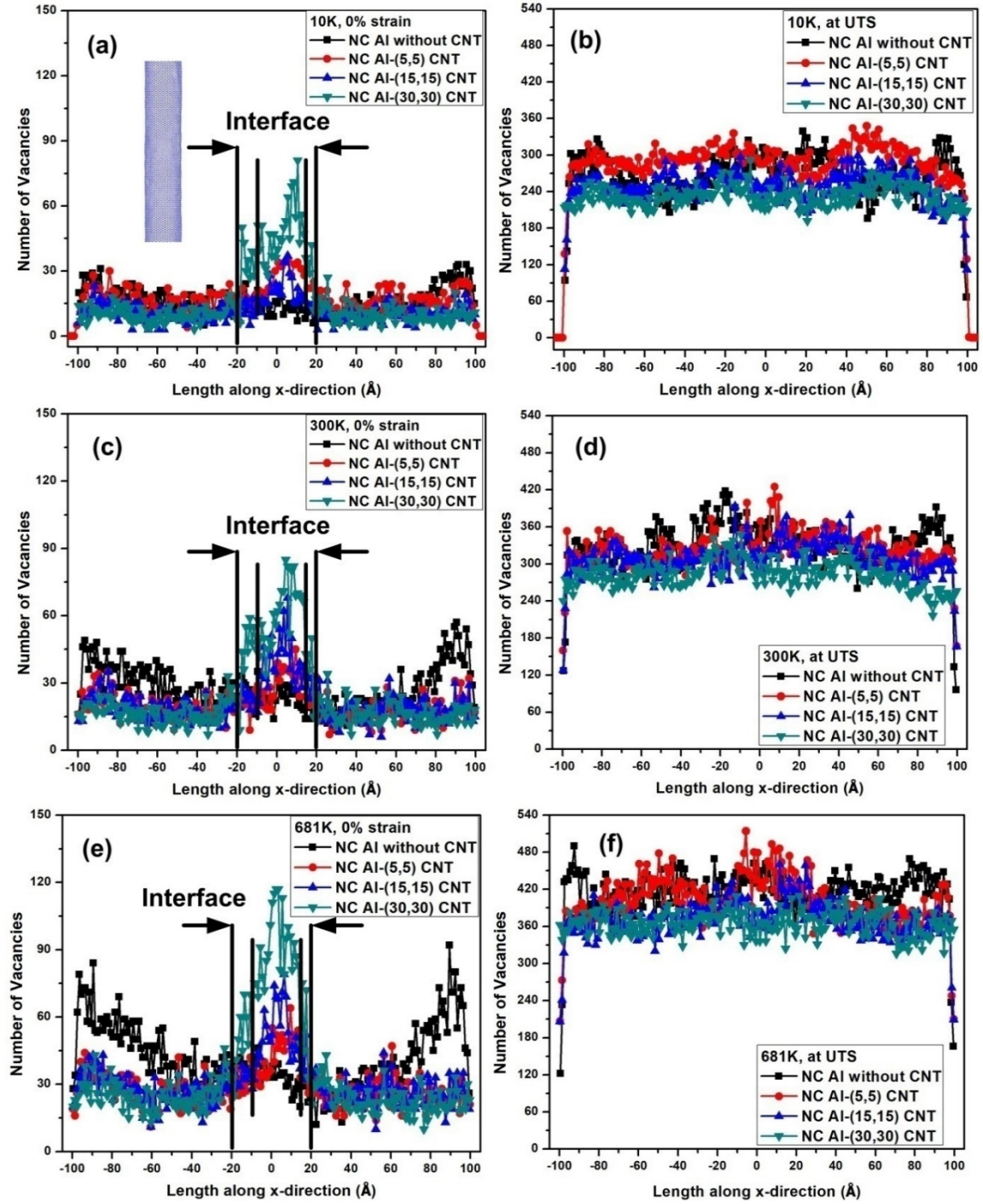
Fig. 11. Plots showing number of vacancies vs. length along x-direction for NC Al without CNT and CNT reinforced NC Al specimens at various temperatures (a) 10 K - 0% strain, (b) 10 K - UTS, (c) 300 K - 0% strain, (d) 300 K - UTS and (e) 681 K - 0% strain, (f) 681 K - UTS.
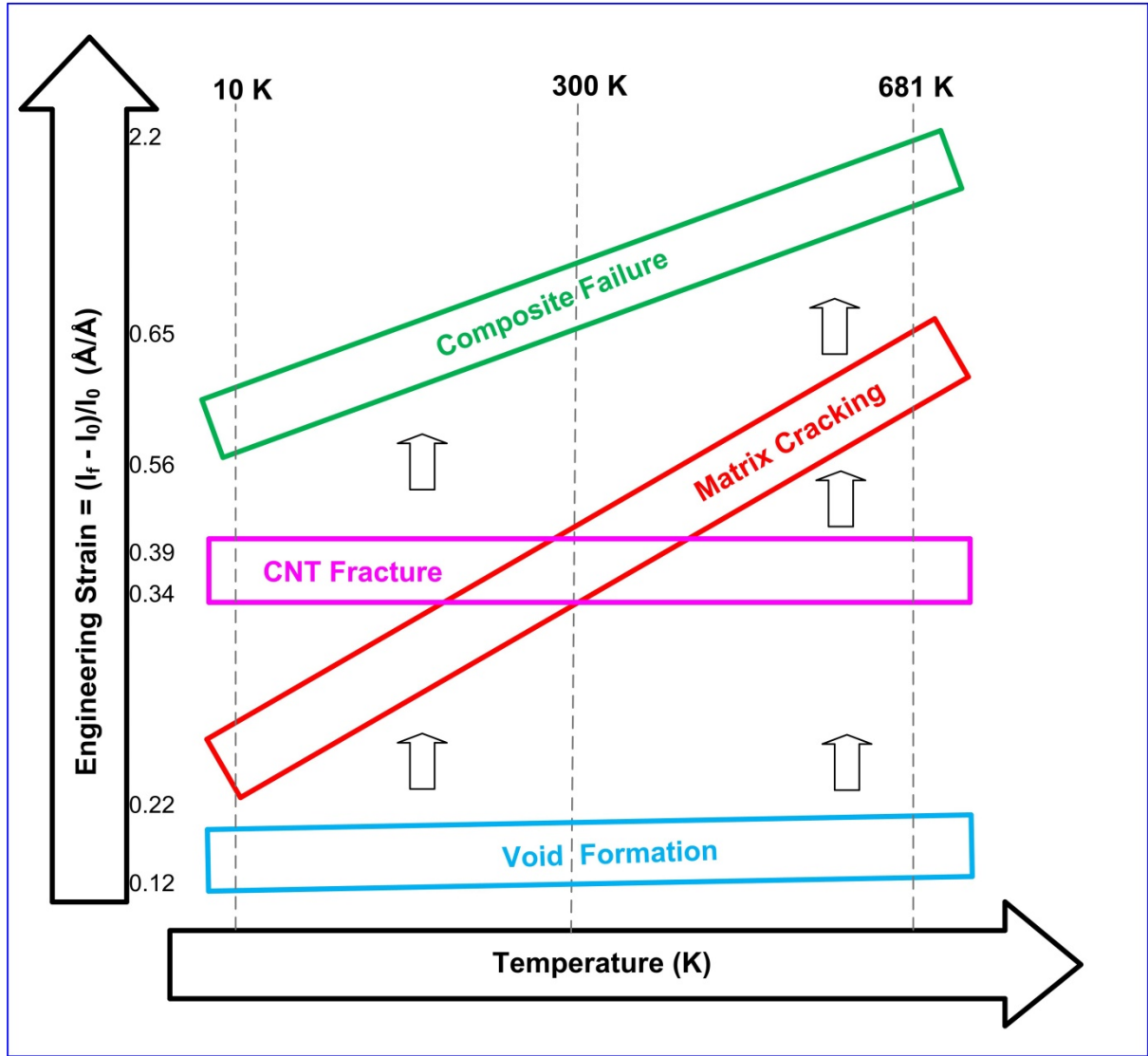
Fig. 12. Dependence of deformation mechanisms on engineering strain and temperature (l_f → final length and l_0 → initial length).

The summary of the deformation mechanisms involved in the present study with respect to temperature and engineering strain is shown **Fig. 12**. Values of strain at which each event initiates have been obtained from the atomic snapshots. Three events, namely, void formation, matrix cracking and CNT fracture have been investigated. It is observed that for all the investigated temperatures, the grain boundaries of the matrix and grain boundary/CNT interfaces are potential sites for void nucleation. This is seen to occur in the strain range of 0.12 to 0.22. Matrix cracking (crack propagation) is seen to take place along the grain boundary through voids amalgamation. Initiation of matrix cracking has been observed at low strains

(ε=~0.22) for low temperatures (~10 K), whereas for high temperatures (~681 K) matrix cracking is initiated at high strains (ε=~0.65). Among the many types of dislocations, Shockley partials contribute to prominent driving deformation for NC Al without CNT and CNT incorporated NC Al specimens. Due to CNT incorporation in NC Al specimens, the dislocation density is higher than in NC Al without CNT. CNT fracture through Stone Wales defect is seen to occur in the strain range 0.34 to 0.39, and is found to be independent of temperature. Overall, the composites have failed in the following manner: the NC Al matrix material is fractured first, then the CNT due to low ductility at low temperatures, whereas at high temperatures, the CNT fractures first followed by the NC Al matrix material.

Conclusions

A MD simulation based study has been carried out to investigate the effect of CNT on the mechanical behaviour of NC Al reinforced CNT composites. It reveals that (30,30) CNT is the best for enhancing the strength and causing delay in fracture for NC Al. In addition, it can also be concluded that the failure is initiated by matrix cracking at low temperature and fibre breakage at high temperature. The behaviour of vacancies at the interface has also been analysed, and we find that the higher concentration of vacancies for higher CNT diameters at the interface is attributed to the higher surface area. These results will help understand the underlying mechanisms leading to the improvement of mechanical properties in NC metals reinforced with CNT.

References

[1] L. Lu, X. Chen, X. Huang, K. Lu, Revealing the maximum strength in nanotwinned copper, Sci. 323(5914) (2009) 607-610.

[2] K. Tanigaki, H. Ogi, H. Sumiya, K. Kusakabe, N. Nakamura, M.Hirao, H. Ledbetter, Observation of higher stiffness in nanopolycrystal diamond than monocrystal diamond, Nat. comm. 4 (2013) 2343.

[3] S. Pal, K. Gururaj, M. Meraj, R.G. Bharadwaj, Molecular Dynamics Simulation Study of Uniaxial Ratcheting Behaviors for Ultrafine-Grained Nanocrystalline Nickel, J. Mat. Eng. Per. 28 (8) (2019) 4918-4930.

[4] C. Suryanarayana, C.C. Koch, Nanocrystalline materials – Current research and future directions, Hyp. Int. 130 (2000) 5-44.

[5] S. Pal, Md. Meraj, C. Deng, Effect of Zr addition on creep properties of ultra-fine grained nanocrystalline Ni studied by molecular dynamics simulation, Comp. Mat. Sci. 126 (2017) 382-392.

[6] D.G. Morris, M.A. Morris, Hardness, strength, ductility and toughness of nanocrystalline materials, In Mat. Sci. For. Trans. Tech. Pub. 235 (1997) 861-872.

[7] S. Pal, S. Mishra, M. Meraj, A.K. Mondal, B.C. Ray, On the comparison of interrupted and continuous creep behaviour of nanocrystalline copper: A molecular dynamics approach, Mat. Let. 229 (2018) 256-260.

[8] X. Shen, J. Lian, Z. Jiang, Q. Jiang, High strength and high ductility of electrodeposited nanocrystalline Ni with a broad grain size distribution, Mat. Sci. Eng. A 487 (1-2) (2008) 410-416.

[9] E. Ma, Instabilities and ductility of nanocrystalline and ultrafine-grained metals, Scr. Mat. 49 (7) (2003) 663-668.

[10] Y.T. Zhu, X. Liao, Nanostructured metals: retaining ductility, Nat. Mat. 3 (6) (2004) 351-352.

[11] C.C. Koch, Optimization of strength and ductility in nanocrystalline and ultrafine grained metals, Scr. Mat. 49 (7) (2003) 657-662.

[12] L.G. Bulusheva, V.I. Sysoev, E.V. Lobiak, Y.V. Fedoseeva, A.A. Makarova, M. Dubois, E. Flahaut, A.V. Okotrub, Chlorinated holey double-walled carbon nanotubes for relative humidity sensors, Car. 148 (2019) 413-420.

[13] A. Muhulet, F. Miculescu, S.I. Voicu, F. Schütt, V.K. Thakur, Y,K, Mishra, Fundamentals and scopes of doped carbon nanotubes towards energy and biosensing applications, Mat. Tod. Ene. 9 (2018) 154-186.

[14] V.R. Raphey, T.K. Henna, K.P.Nivitha, P. Mufeedha, C. Sabu, K. Pramod, Advanced biomedical applications of carbon nanotube, Mat. Sci. Eng: C 100 (2019) 616-630.

[15] S. Li, Y. Yao, Synergistic improvement of epoxy composites with multi-walled carbon nanotubes and hyperbranched polymers, Com. Par. B: Eng. 165 (2019) 293-300.

[16] R. Calderón-Villajos, A.J. López, L. Peponi, J. Manzano-Santamaría, A. Ureña, 3D-printed self-healing composite polymer reinforced with carbon nanotubes, Mat. Let. 249 (2019) 91-94.

[17] G. Lee, M. Sung, J.H. Youk, J. Lee, W.R. Yu, Improved tensile strength of carbon nanotube-grafted carbon fiber reinforced composites, Comp. Str. 220 (2019) 580-591.

[18] H. Yao, G. Zhou, W. Wang, M. Peng, Effect of polymer-grafted carbon nanofibers and nanotubes on the interlaminar shear strength and flexural strength of carbon fiber/epoxy multiscale composites, Comp. Stru. 195 (2018) 288-296.

[19] A.Y. Boroujeni, M. Al-Haik, Carbon nanotube–Carbon fiber reinforced polymer composites with extended fatigue life, Comp. Par. B: Eng. 164 (2019) 537-545.

[20] Q. Shen, Q. Song, H. Li, C. Xiao, T. Wang, H. Lin, W. Li, Fatigue strengthening of carbon/carbon composites modified with carbon nanotubes and silicon carbide nanowires, Int. J. Fat. 124 (2019) 411-421.

[21] H.J. Choi, D.H. Bae, Strengthening and toughening of aluminum by single-walled carbon nanotubes, Mat. Sci. Eng. A 528 (6) (2011) 2412-2417.

[22] A. Agarwal, S.R. Bakshi, D. Lahiri, Carbon nanotubes: reinforced metal matrix composites, CRC Press, Boca Raton, 2018.

[23] Y. Shi, L. Zhao, Z. Li, Z. Li, D.B. Xiong, Y. Su, S. Osovski, Q. Guo, Strengthening and deformation mechanisms in nanolaminated single-walled carbon nanotube-aluminum composites, Mat. Sci. Engg. A 764 (2019) 138273.

[24] J. Hou, W. Du, G. Parande, M. Gupta, S. Li, Significantly enhancing the strength+ ductility combination of Mg-9Al alloy using multi-walled carbon nanotubes. J. All. Comp. 790 (2019) 974-982.

[25] S.R. Bakshi, D. Lahiri, A. Agarwal, Carbon nanotube reinforced metal matrix composites-a review, Int. Mat. Rev. 55 (1) (2010) 41-64.

[26] B. Duan, Y. Zhou, D. Wang, Y. Zhao, Effect of CNTs content on the microstructures and properties of CNTs/Cu composite by microwave sintering, J. All. Comp. 771 (2019) 498-504.

[27] D.H. Nam, S.I. Cha, B.K. Lim, H.M. Park, D.S. Han, S.H. Hong, Synergistic strengthening by load transfer mechanism and grain refinement of CNT/Al–Cu composites, Car. 50 (7) (2012) 2417-2423.

[28] K.V. Reddy, C. Deng, S. Pal, Dynamic characterization of shock response in crystalline-metallic glass nanolaminates, Acta Mat. 164 (2019) 347-361.

[29] M. Meraj, N. Yedla, S. Pal, The effect of porosity and void on creep behavior of ultra-fine grained nano crystalline nickel, Mat. Let. 169 (2016) 265-268.

[30] B.K. Choi, G.H. Yoon, S. Lee, Molecular dynamics studies of CNT-reinforced aluminum composites under uniaxial tensile loading, Comp. Par. B: Eng. 91 (2016) 119-125.

[31] J. Xiang, L. Xie, S.A. Meguid, S. Pang, J. Yi, Y. Zhang, R. Liang, An atomic-level understanding of the strengthening mechanism of aluminum matrix composites reinforced by aligned carbon nanotubes, Comp. Mat. Sci. 128 (2017) 359-372.

[32] Z.W. Xue, L.D. Wang, P.T. Zhao, S.C. Xu, J.L. Qi, W.D. Fei, Microstructures and tensile behavior of carbon nanotubes reinforced Cu matrix composites with molecular-level dispersion, Mat. Des. 34 (2012) 298-301.

[33] N. Silvestre, B. Faria, J.N.C. Lopes, Compressive behavior of CNT-reinforced aluminum composites using molecular dynamics. Comp. Sci. Tech. 90 (2014) 16-24.

[34] K. Duan, L. Li, Y. Hu, X. Wang, X. Damping characteristic of Ni-coated carbon nanotube/copper composite. Mat. Des. 133 (2017) 455-463.

[35] B. Chen, K. Kondoh, H. Imai, J. Umeda, M. Takahashi, Simultaneously enhancing strength and ductility of carbon nanotube/aluminum composites by improving bonding conditions, Scr. Mat. 113 (2016) 158-162.

[36] D. Chen, Structural modeling of nanocrystalline materials, Comp. Mat. Sci. 3 (3) (1995) 327-333.

[37] P. Hirel, Atomsk: a tool for manipulating and converting atomic data files, Comp. Phy. Comm. 197 (2015) 212-219.

[38] Y. Mishin, D. Farkas, M.J. Mehl, D.A. Papaconstantopoulos, Interatomic potentials for monoatomic metals from experimental data and ab initio calculations, Phy. Rev. B 59 (5) (1999) 3393.

[39] S.J. Stuart, A.B. Tutein, J.A. Harrison, A reactive potential for hydrocarbons with intermolecular interactions, J. Che. Phy. 112 (14) (2000) 6472-6486.

[40] C.R. Dandekar, Y.C. Shin, Molecular dynamics based cohesive zone law for describing Al–SiC interface mechanics, Comp. Par. A: App. Sci. Manf. 42 (4) (2011) 355-363.

[41] S. Plimpton, Fast parallel algorithms for short-range molecular dynamics, J. Comp. Phy. 117 (1) (1995) 1-19.

[42] A. Stukowski, Visualization and analysis of atomistic simulation data with OVITO–the Open Visualization Tool, Mod. Sim. Mat. Sci. Eng. 18 (1) (2009) 015012.

[43] A. Stukowski, V.V. Bulatov, A. Arsenlis, Automated identification and indexing of dislocations in crystal interfaces, Mod. Sim. Mat. Sci. Eng. 20 (8) (2012) 085007.

[44] J.D. Honeycutt, H. C. Andersen, Molecular dynamics study of melting and freezing of small Lennard-Jones clusters, J. Phy. Che. 91 (19) (1987) 4950-4963.

[45] M.L. Falk, J.S. Langer, Dynamics of viscoplastic deformation in amorphous solids, Phy. Rev. E 57 (6) (1998) 7192.

[46] F. Shimizu, S. Ogata, J. Li, Theory of shear banding in metallic glasses and molecular dynamics calculations, Mat. Trans. 48 (11) (2007) 2923-2927.

[47] M. Jafari, M.H. Abbasi, M.H. Enayati, F. Karimzadeh, Mechanical properties of nanostructured Al2024–MWCNT composite prepared by optimized mechanical milling and hot pressing methods, Adv. Pow. Tech. 23 (2) (2012) 205-210.

[48] W. Xu, L.P. Davila, Size dependence of elastic mechanical properties of nanocrystalline aluminum, Mat. Sci. Engg: A, 692 (2017) 90-94.

[49] P.C. Tsai, Y.R. Jeng, J.T. Lee, I. Stachiv, P. Sittner, Effects of carbon nanotube reinforcement and grain size refinement mechanical properties and wear behaviors of carbon nanotube/copper composites, Dia. Rel. Mat. 74 (2017) 197-204.

[50] H.J. Choi, B.H. Min, J.H. Shin, D.H. Bae, Strengthening in nanostructured 2024 aluminum alloy and its composites containing carbon nanotubes, Comp. Par. A: App. Sci. Manf. 42 (10) (2011) 1438-1444.

[51] D. Chunfeng, X. Zhang, M.A. Yanxia, W. Dezun, Fabrication of aluminum matrix composite reinforced with carbon nanotubes, Rare Met. 26 (5) (2007) 450-455.

[52] Z.Y. Liu, B.L. Xiao, W.G. Wang, Z.Y. Ma, Tensile strength and electrical conductivity of carbon nanotube reinforced aluminum matrix composites fabricated by powder metallurgy combined with friction stir processing. J. Mat. Sci. Tech. 30 (7) (2014) 649-655.

[53] F. Ostovan, K.A. Matori, M. Toozandehjani, A. Oskoueian, H.M. Yusoff, R. Yunus, A.H.M. Ariff, H.J. Quah W.F. Lim, Effects of CNTs content and milling time on mechanical behavior of MWCNT-reinforced aluminum nanocomposites. Mat. Chem. Phy. 166 (2015) 160-166.

[54] H. Kwon, M. Estili, K. Takagi, T. Miyazaki, A. Kawasaki, Combination of hot extrusion and spark plasma sintering for producing carbon nanotube reinforced aluminum matrix composites. Car. 47 (3) (2009) 570-577.

[55] H. Kwon, D.H. Park, J.F. Silvain, A. Kawasaki, Investigation of carbon nanotube reinforced aluminum matrix composite materials. Comp. Sci. Tech. 70 (3) (2010) 546-550.

[56] D. Hull and D.J. Bacon, Introduction to Dislocations, Butterworth-Heinemann, Oxford, 2001.

[57] A.G. Frøseth, P.M. Derlet, H. Van Swygenhoven, Dislocations emitted from nanocrystalline grain boundaries: nucleation and splitting distance. Acta Mat. 52 (20) (2004) 5863-5870.

[58] P.M. Derlet, A. Hasnaoui, H. Van Swygenhoven, Atomistic simulations as guidance to experiments. Scr. Mat. 49 (7) (2003) 629-635.

[59] Y.B. Lu, Q.S. Yang, X.Q. He, K.M. Liew, Modeling the interfacial behavior of carbon nanotube fiber/polyethylene composites by molecular dynamics approach, Comp. Mat. Sci. 114 (2016) 189-198.

[60] M. Chen, E. Ma, K.J. Hemker, H. Sheng, Y. Wang, X. Cheng, Deformation twinning in nanocrystalline aluminium, Sci. 300 (5623) (2003) 1275-1277.

[61] J. P. Hirth and J. Lothe, Theory of Dislocations, Krieger Publishing, Malabar, U.K., 1992, 2nd ed.

[62] Q. Lu, B. Bhattacharya, Effect of randomly occurring Stone–Wales defects on mechanical properties of carbon nanotubes using atomistic simulation, Nanotech. 16 (4) (2005) 555.

[63] G. Wilde, S. Divinski, Grain Boundaries and Diffusion Phenomena in Severely deformed Materials, Mat. Trans. 60 (7) (2019) 1302-1315.